euspen's 23rd International Conference & Exhibition, Copenhagen, DK, June 2023
www.euspen.eu

Evaluation of surface roughness and periodical layers in material jetting

Ali Payami Golhin[1,*], Aditya Suneel Sole[2], Are Strandlie[1]

[1] *Department of Manufacturing and Civil Engineering, Norwegian University of Science and Technology, 2815 Gjøvik, Norway*
[2] *Department of Computer Science, Norwegian University of Science and Technology, 2815 Gjøvik, Norway*

**ali.p.golhin@ntnu.no*

Abstract

Studying surface texture and morphology is essential to developing Additive Manufacturing (AM). Assessing the quality of part layer compounds in the process will assist with adjusting process parameters for optimal part quality in the manufacturing process. For this purpose, Material Jetting (MJT) system has been used to manufacture objects at various platform locations (swathes) to examine the surface morphology, including surface roughness and texture. Due to the rotating disc used as the build platform, the studied parts showed a different surface morphology from parts printed using other material jetting machines. To study the surface texture, we generated high-resolution surface mesh grids after scanning the surface using a coordinate measuring machine (CMM) and a 3D scanner. The surface topography was decomposed into scan lines using a fast Fourier transform (FFT). The power spectral density (PSD) of a surface was calculated and compared to roughness to discuss the surface topography. Signal processing demonstrated that different textures can be fabricated by tuning the printing position conditions. As a result of determining the surface texture and roughness characteristics in conjunction with 3D printing parameters in the design process, it was possible to categorize the build platform regions based on their surface textures.

Keywords: Additive manufacturing, Material Jetting, Texture, Object appearance

1. Introduction

Material Jetting (MJT), as reported in the ISO/ASTM 52900:2015, fabricates objects by jetting materials onto a build platform in either a Drop on Demand (DOD) or continuous manner. The jetting process is similar to that of a standard inkjet printer. PolyJet, Multi Jet Printing (MJP), Objet, and XJet's NanoParticle Jetting (NPJ) are the fundamental processes in MJT. Thanks to high-resolution MJT 3D printers, manufactured objects show detailed appearance attributes, such as texture, color, gloss, and gonio-chromatic effects [1, 2].

MJT-based products not only depose resins in CMYKW (cyan, magenta, yellow, black, and white) but can also print different materials. It is now possible to 3D print MJT materials with vastly different properties, such as a rigid, glassy polymer and a soft, rubbery material with elastic moduli that differ by nearly three orders of magnitude at room temperature [1]. Therefore, MJT has been adopted to produce a wide range of prototypes with complex shapes and appearances, as well as functional polymers such as scaffolds for tissue engineering, multi-material structures, and memory shape polymers for 4D printing [3]. MJT objects are semi-translucent, complicated in appearance, and represent a mixture of textures by applying ink in layers [2]. Thus, the detailed properties are difficult to capture by conventional methods. Still, it is possible to achieve satisfying results by decreasing the influence of errors in the measurement process and following a reproducible workfellow.

Some of the MJT printers, such as the Stratasys J55, use a rotary disc as the build platform for 3D printing. The rotating tray decreases the size of the MJT 3D printer, which allows it to be used at home or in an office due to the reduced dimensions. However, it impacts surface morphology and appearance. The spatial frequency components of additively manufactured surfaces include texture profile, form, waviness, and roughness [4]. Each of these components has a unique origin and influences the appearance and functionality of the product distinctly. The waviness may indicate machine vibration. The form is typically the result of poor manufacturing system performance, and the profile can be identified by layer-by-layer manufacturing. In contrast, surface irregularities caused by printing and material removal errors generate roughness [5]. Considering surface morphology is essential in creating functional surfaces such as super-hydrophobic and super-hydrophilic surfaces, surfaces with structural colors, and bio-inspired/bio-mimetic surfaces [6]. Accordingly, the role of surface textures in 3D-printed polymers has been studied and addressed for tribological behavior [7] and biomechanical [8].

Although the appearance of 3D-printed parts is qualitative, subjective, and controversial [9, 10], instrumental texture measurements can be used to indirectly evaluate the performance of AM methods based on their topography as a quality control concept [11].

The coordinate-measuring machine (CMM) is a valuable tool used to measure the geometrical characteristics of physical objects [12]. Holmberg et al. [13] investigated the changes in surface morphologies during machining using optical microscopy and full width at half maximum (FWHM) assessment. Texture evaluation enables the reconstruction of AM profile and the execution of appearance evaluation and data registration. Fast Fourier Transform (FFT) analysis filters out high-frequency waves to uncover the underlying signal. Calta et al. [14] employed the 1D FFT of the line profile of track height to measure the periodicity of surface characteristics, ignoring the start and end of the scanning track to eliminate inaccuracies produced by boundary effects.

In this context, the structure of the study aims to present a novel approach to studying surface morphology by investigating texture profiles and surface roughness on MJT surfaces. The procedure described in the next section as the experimental procedure, involves 3D scanning, optical profilometry, and CMM testing. A rotary MJT system has been used to manufacture objects at different platform locations (swathes). The outcome of the experiments has been presented in the results and discussion section. It opens opportunities for high-quality structures through high-fidelity printing and reduces the post-processing requirement, as discussed in the conclusion section.

2. Experimental procedure

Specimens were created using acrylate-based materials and photoinitiators in a Stratasys J55 3D printer. A J55 placement zone comprises three equal-width areas: inner, middle, and outer (see Figure 1A). For optimal placement and faster construction, the innermost side of the rotary disc should be used first. The influence of printing location (swath) on the texture formation is investigated using a full factorial experimental design. For this purpose, nine specimens, including three parts for each swath, were manufactured in sizes of 60 × 13 × 3.5 mm for texture evaluation and 3D scanning, as well as 40 × 30 × 3.5 mm for roughness measurements. White as-printed parts with a glossy on matte (GoM) finish between the colored and white layer were selected for 3D scanning (Figure 1B).

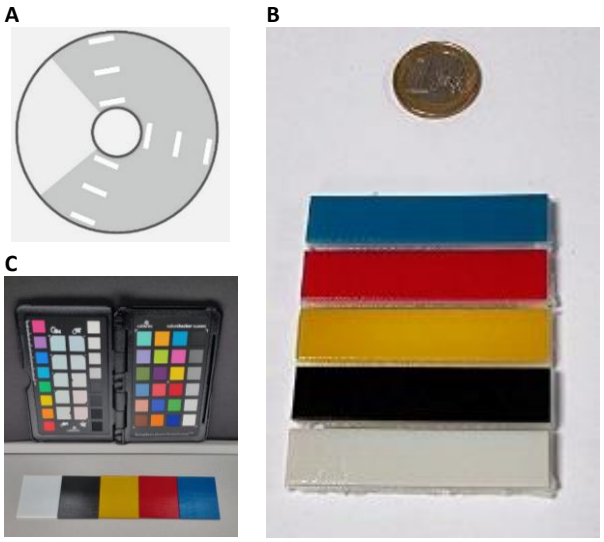

Figure 1A. Rotary build platform and parts positions on three different swaths, **B.** as-printed specimens for texture evaluation, and **C.** trial specimens for 3D scanning (scale bar 10 mm).

Specimens have been scanned in width (Z-axis) and length (X-axis) directions (Figure 2B) using a ZEISS DuraMax CMM machine equipped with ZEISS VAST XXT tactile scanning probe and ZEISS CALYPSO 2021 software. The measurement was conducted with a step width of 20 µm, a probe radius of 1.5 mm, and 2.4 µm accuracy in the measuring length of 30 mm in XYZ directions. A desktop 3D scanner (AutoScan Inspec, Shining 3D) was used in a dimmed condition. The samples were mounted on a turntable and rotated eight times, once every 45°, to provide a 360° panorama. Using a projector that produced structured light patterns allowed a scanning accuracy of 10 µm. Two 5.0-megapixel CCD cameras are installed in the scanner and used to measure distorted sizes. Multiple scans from different angles are used to compile the registered point cloud. After combining the scans in UltraScan 2022, the model was exported in OBJ format to SolidWorks Visualize (v2021). A Keyence VH-ZST microscope (20X to 2000X) is used to measure the surface roughness and display surface morphology.

Results from the CMM were compared with the object's 3D coordinates in the computer-aided design (CAD) part. Once the CMM data was gained, it was processed in Gwyddion (v2.59) to calculate the layer heights, thicknesses, and topography. To investigate the height distribution, we employed FWHM, the width measured at the half level between the peak of the line and the continuum, using the Gauss function to fit the height distribution curve. OriginPro v9.5 was employed for data analysis.

ISO 11562 [15] specifies the use of a 1D Gaussian filter to extract surface contour reference lines by a weight function, *s(x)*, defined as follows

$$s(\mathrm{x}) = \frac{1}{\alpha\lambda_c}\exp\left(-\pi\left(\frac{x}{\alpha\lambda_c}\right)^2\right) \qquad (1)$$

where *x* is a spatial domain variable as the distance from the maximum of *s(x)*, λ_c is the cutoff wavelength, and the constant value of α delivers 50 % transmission characteristic at λ_c. The equations below show that the power output is normalized as the space-integral squared amplitude (TISA), where time represents space in standard annotations.

$$P_{xx}\left(e^{j\omega}\right) = \sum_{m=-\infty}^{\infty} r_{xx}(m)e^{-j\omega m} \qquad (2)$$

$$TISA\ (Power) = \frac{\Delta t\left({R_e}^2+{I_m}^2\right)}{n} \qquad (3)$$

where $P_{xx}\left(e^{j\omega}\right)$ is the spectrum or power density (PSD), $r_{xx}(m)$ acts as the auto-correlation function for the response signal, Δt is the sampling interval, R_e and I_m are the real and imaginary elements of the transform data, and *n* is considered as the length of the response sequence. The following function is used to mitigate leakage.

$$N/\sum_{n=0}^{N-1} w(n)^2 \qquad (4)$$

where $w(n) = 1$ for $0 \le n \le N-1$, and 0 for the other range.

3. Results and Discussion

J55 printers produce rigid, brittle 3D-manufactured components that are slightly bent over a short period [2]. As shown in our previous study [16], a closer examination of the several built models reveals some minor damage and glue to the pieces. As shown in Figure 2A, the semicircle pattern is visible in the surface texture images associated with the 3D-printed layers. Therefore, the scanning strategy is crucial for establishing the appropriate traceability of measurements on CMMs (Figure 2B).

Figure 2C depicts the 3D view of the printed surface after rasterization. Analysis of the XYZ coordination indicates that the distribution of Z heights of the surface asperities is less than 17 µm. As a result of the slight bending of the parts that typically occurs a few days after printing, which was observed in our previous work [9, 16], there is a concentration of missed scanned meshes in the middle of the models. This can be attributed to possible post-curing exposure to natural light.

High-resolution optical images of the specimens can be seen in Figure 3. The glossy and translucent appearance of MJT products, along with the curvature resulting from UV absorbance during storage, make it difficult to study them using

an optical profilometer (see Figure 3A). The mean parameters of the area roughness in Table 1 were calculated based on the surface topography analysis on a region of 2.5 × 2.5 (mm), as shown in Figure 3B.

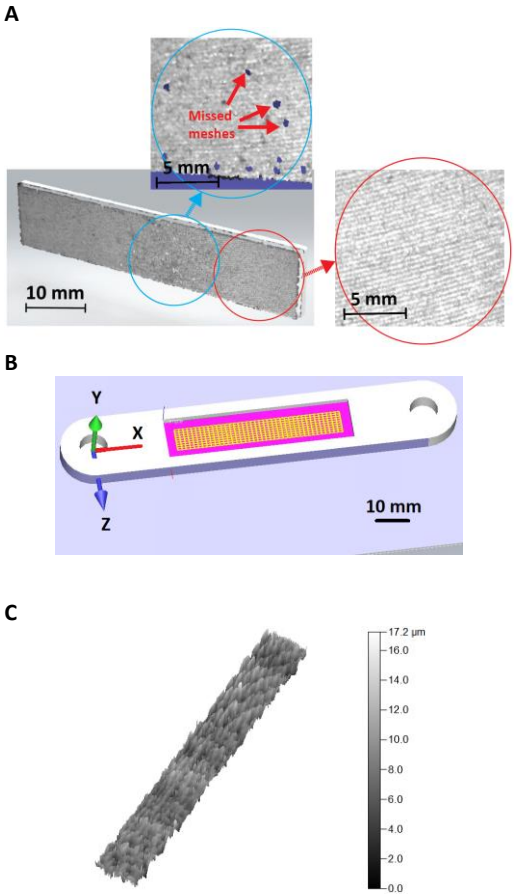

Figure 2A. 3D-scanned model of the printed parts, **B.** CMM setup for the contact scanning strategy (yellow grid) on the scanned area (purple area). A specific sample holder (the piece in white) is 3D-printed to decrease the bending effect through the length of the specimens. **C.** 3D model of the surface morphology through the CMM-scanned area, with the exaggerated scale bars showing the height distributions over height direction.

According to Table 1, MJT can produce an exceptionally smooth surface. The surface roughness was influenced by the location of printing on the build platform. The smoothest surface was obtained in the middle swath (S_a=1.02 µm), followed by the outer (S_a=1.16 µm) and the inner (S_a=1.65 µm) swaths. Due to the slightly positive skewness (S_{sk}) values of all specimens, there were more peaks and asperities than valleys on the surfaces. As a result of high kurtosis (S_{ku}), these profile peaks were slightly sharp.

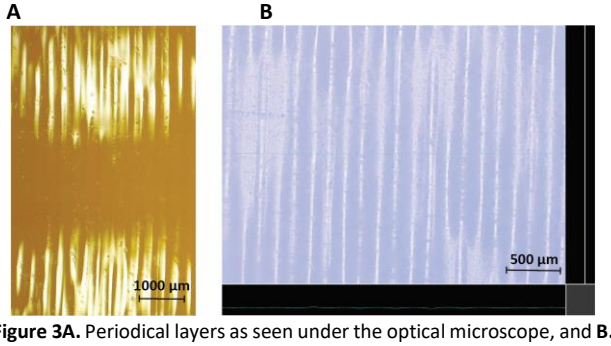

Figure 3A. Periodical layers as seen under the optical microscope, and **B.** selected surface area for roughness measurement.

Table 1 Mean surface roughness results

	Area roughness parameter*			
Swath	**S_a (µm)**	**S_q (µm)**	**S_{sk}**	**S_{ku}**
Inner	1.65	2.21	0.15	3.2
Middle	1.02	1.42	0.03	2.2
Outer	1.16	1.90	0.08	2.9

* S_a: Height deviations from the Mean Reference Plane of the measurement area (A); S_q: Root mean square of surface heights; S_{sk}: the skewness and S_{ku}: the kurtosis of the surface

Figure 4A depicts the FFT analysis applied to height grids and a deeper look at additively built layers generated using CMM data (Z height). It indicates FWHM and the mean layer height of different swaths display a meaningful correlation, in which FWHM (3.8 µm) and the minimum arithmetic means of layer height (5.7 µm) were within the middle swath. Figure 4B shows clear peaks for the averaged data, validating the periodicity of the layers and their related surface texture in the investigated parts. Averaging the distances between the PSD peaks gives an arithmetic mean of the periodic gap between layers. According to Figure 4C, as the radius of the build location increases, thinner layers result from 305 µm to 303 µm. An increased centrifugal force on the outer region of the disc allows the printhead to build closer layers as it moves from the inner to the outer edge of the tray. However, CMM results for mean layer height and FWHM in Figure 4C followed the same trend as the roughness measurement results in Table 1.

4. Conclusions

This morphology study was conducted on the surface roughness and texture of polymer parts manufactured by material jetting technology. It provided a method for determining the surface morphology and appearance of components printed on various areas of a rotary disc tray as a build platform. CMM results indicated the minimum arithmetic mean (5.7 µm) and maximum FWHM (3.8 µm) of Z height values were within the middle swath, indicating a meaningful trend in the swath selection. The optical profilometry surface roughness results followed the same trend, with the lowest roughness observed in the middle swath and the roughest in the inner swath. The PSD results confirmed the periodicity of the layers and determined their widths. As the print head moved from the inner to the outer area, the thickness of the layer decreased from 305 µm to 303 µm, and closer layers were printed. This can be due to increased centrifugal forces along the radius of the disc. Accordingly, the middle swath on the build platform produced smoother surfaces. However, it required more time to print in this area than in the inner swath. Implementing 3D printing technology under optimized conditions resulted in parts with enhanced surface quality in the middle swath. Since the MJT technology with a rotary tray now makes it possible to create prototypes for home and office use, these findings can lead to a better knowledge of the surface texture in these printers and fewer post-processing operations.

Acknowledgments

The authors appreciate the support provided by Dr. Andreas Kraushaar (Fogra Forschungsinstitut für Medientechnologien e.V.) and Donatela Saric (NTNU & Fogra) for the roughness measurement. This work is funded by the European Union's H2020 research and innovation program under the Marie Skłodowska-Curie grant agreement No. 814158 "ApPEARS - Appearance Printing - European Advanced Research School".

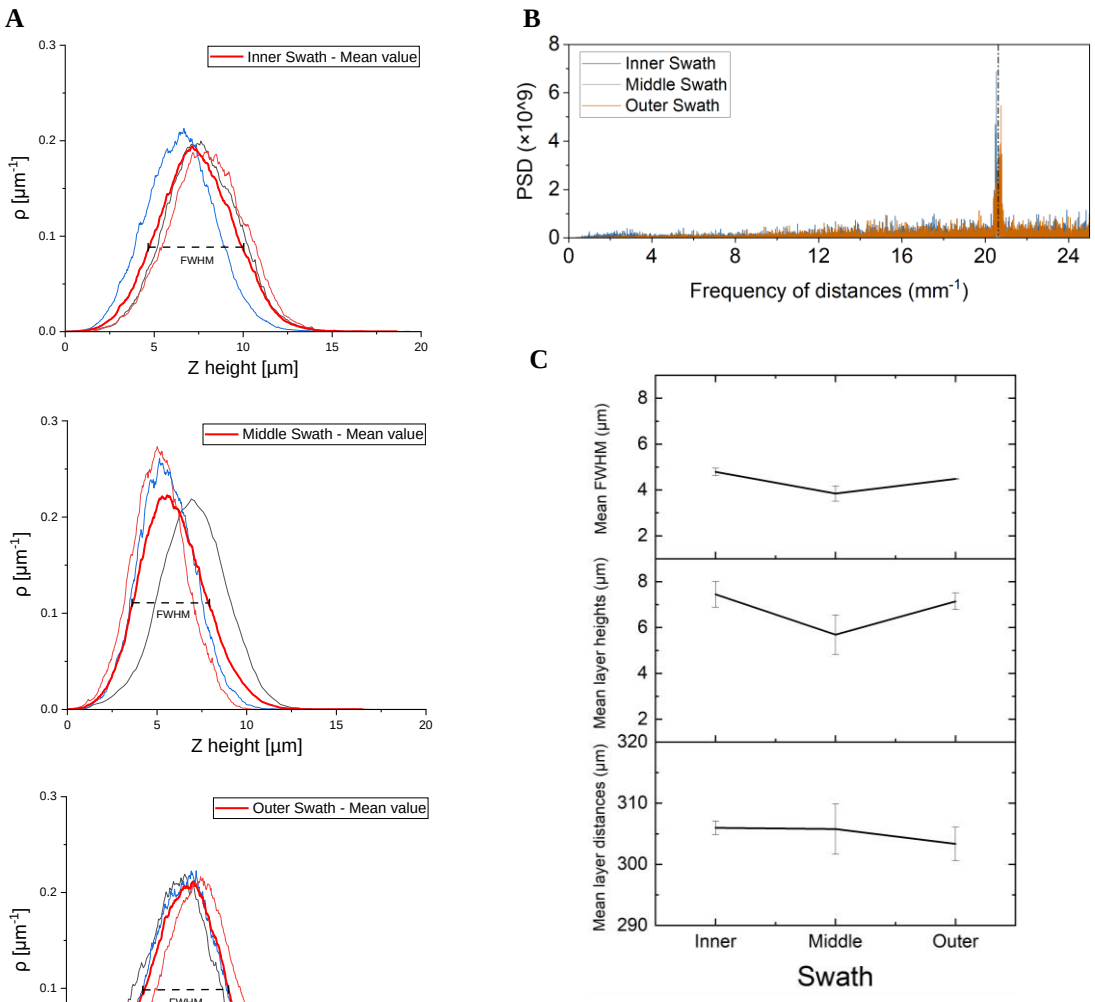

Figure 4A. Z height distribution profile for parts manufactured at different swaths, **B.** PSD results over the scanned profile, and **C.** periodic texture characteristics.

References

[1] De Noni L, Zorzetto L, Briatico-Vangosa F, et al. 2022 Modelling the interphase of 3D printed photo-cured polymers *Compos. B. Eng.* **234** 109737

[2] Golhin AP, Sole AS, Strandlie A 2023 Color appearance in rotational material jetting *Int. J. Adv. Manuf. Technol*. **124** 1183

[3] Khoo ZX, Teoh JEM, Liu Y, et al. 2015 3D printing of smart materials: A review on recent progresses in 4D printing *Virtual Phys. Prototyping* **10** 103

[4] Payami Golhin A 2021 Generation of micro-and nano-textured surfaces *European Commission: Brussels*. 1

[5] Du S, Liu C, Huang D 2015 A shearlet-based separation method of 3D engineering surface using high definition metrology *Precis. Eng.* **40** 55

[6] Afshar-Mohajer M, Zou M 2020 Multi-Scale In Situ Tribological Studies of Surfaces with 3D Textures Fabricated via Two-Photon Lithography and Replica Molding *Adv. Mater. Interfaces* **7** 2000299

[7] Luo M, Huang S, Man Z, et al. 2022 Tribological behaviour of fused deposition modelling printed short carbon fibre reinforced nylon composites with surface textures under dry and water lubricated conditions *Friction* **10** 2045

[8] Lindsay C, Ruppert D, Abumoussa S, et al. 2020 Benefits of additive manufacturing and micro and nano surface texture modifications on mechanical strength and infection resistance of skin–implant interfaces in rats. *J. Biomater. Appl* **0** *1*

[9] Payami Golhin A, Srivastava C, Tingstad JF, et al. 2022 Additive manufacturing of multilayered polymer composites: Durability assessment *Proceedings of the 20th European Conference on Composite Materials-Composites Meet Sustainability* EPFL Lausanne, Switzerland **6**

[10] Yuan J, Chen G, Li H, et al. 2021 Accurate and Computational: A review of color reproduction in Full-color 3D printing *Mater. Des.* **209** 1

[11] Payami Golhin A, Strandlie A, John Green P 2021 The influence of wedge angle, feedstock color, and infill density on the color difference of FDM objects. *J. Imaging Sci. Technol.* **65** 1

[12] Anadioti E, Kane B, Zhang Y, et al. 2022 Accuracy of Dental and Industrial 3D Printers *J. Prosthodont.* **31** 30

[13] Holmberg J, Berglund J, Wretland A, et al. 2019 Evaluation of surface integrity after high energy machining with EDM, laser beam machining and abrasive water jet machining of alloy 718 *Int. J. Adv. Manuf. Technol.* **100** 1575

[14] Calta NP, Martin AA, Hammons JA, et al. 2020 Pressure dependence of the laser-metal interaction under laser powder bed fusion conditions probed by in situ X-ray imaging *Addit. Manuf.* **32** 101084

[15] Geometrical product specifications (GPS) — Surface texture: Areal — Part 2: Terms, definitions and surface texture parameters 2012 *ISO* **25178-2** 1

[16] Payami Golhin A, Srivastava C, Strandlie A, et al. 2023 Effects of accelerated aging on the appearance and mechanical performance of materials jetting products *Mater. Des.* In Press 111863